The oocyte zinc transporter *Slc39a10/Zip10* is a regulator of zinc sparks during fertilization in mice.

Atsuko Kageyama[1], Narumi Ogonuki[2], Takuya Wakai[3], Takafumi Namiki[1,4], Yui Kawata[1], Manabu Ozawa[5], Yasuhiro Yamada[6], Toshiyuki Fukada[7], Atsuo Ogura[2], Rafael A. Fissore[8], Naomi Kashiwazaki[1,9], Junya Ito[1,9,10*]

[1] Laboratory of Animal Reproduction, School of Veterinary Medicine, Azabu University, Sagamihara, 252-5201, Japan.

[2] Bioresource Engineering Division, Bioresource Research Center, RIKEN, Tsukuba, 305-0074, Japan.

[3] Department of Animal Science, Graduate School of Environmental and Life Science, Okayama University, Okayama, 700-8530, Japan.

[4] Present address: Department of Life Science Frontiers, Center for iPS Cell Research and Application (CiRA), Kyoto University, Kyoto, 606-8507, Japan.

[5] Laboratory of Reproductive Systems Biology, Center for Experimental Medicine and Systems Biology, The Institute of Medical Science, The University of Tokyo, Minato-ku 108-8639, Japan.

[6] Department of Molecular Pathology, Graduate School of Medicine, The University of Tokyo, Bunkyo-ku 113-0033, Japan.

[7] Laboratory of Molecular and Cellular Physiology, Faculty of Pharmaceutical Sciences, Tokushima Bunri University, Tokushima 770-8514, Japan.

[8] Department of Veterinary and Animal Sciences, University of Massachusetts Amherst, Amherst 01003-9292, the United States.

[9] Graduate School of Veterinary Science, Azabu University, Sagamihara, 252-5201, Japan.

[10] Center for Human and Animal Symbiosis Science, Azabu University, Sagamihara, 252-5201, Japan.

*Correspondence:

Junya Ito, Laboratory of Animal Reproduction, Graduate School of Veterinary Sciences, Azabu University, Sagamihara, 252-5201, Japan, itoj@azabu-u.ac.jp

Abstract

In all vertebrates studied to date, a rise(s) in intracellular calcium is indispensable for successful fertilization and further embryonic development. Recent studies demonstrated that zinc is ejected to the extracellular milieu, the 'zinc spark', and

follows the first few calcium rises of fertilization. However, the role of the zinc sparks in fertilization and development, and the supporting influx mechanism(s) are unknown. In this study, we focused on zinc transporters *Zip6/Slc39a6* and *Zip10/Slc39a10* both of which are expressed in mouse oocytes through follicular development, and investigated the oocyte-specific deficient mice for *Zip6* (*Zip6*$^{d/d}$: *Zip6*$^{flox/flox}$ *Gdf9*$^{Cre/+}$) and *Zip10* (*Zip10*$^{d/d}$: *Zip10*$^{flox/flox}$ *Gdf9*$^{Cre/+}$). *Zip10* mRNA or ZIP10 protein was expressed throughout folliculogenesis in the oocyte or plasma membrane, respectively. ZIP6 protein was also expressed in the nuclear localization in the oocytes and granulosa cells throughout folliculogenesis. The number of ovulated oocytes was examined in *Zip6*$^{d/d}$ and *Zip10*$^{d/d}$ mice, and no change from the number of oocytes was observed for either strain. *Zip10*$^{d/d}$ oocytes decreased zinc level in the oocytes, but did not affect maturation and metaphase II spindles formation. The levels of zinc fluorescence intensity in the *Zip6*$^{d/d}$ oocytes were not different from the *Zip6*$^{f/f}$ oocytes. Fertilization-induced calcium oscillations were present in both *Zip6*$^{d/d}$ and *Zip10*$^{d/d}$ oocytes, but zinc sparks were not observed in *Zip10*$^{d/d}$ oocytes. Despite other events of egg activation proceeding normally in *Zip10*$^{d/d}$ oocytes, embryo development into 4-cells and beyond was compromised. We show here for the first time that the zinc transporter ZIP10 contributes to zinc homeostasis in oocytes and embryos, highlighting the role of labile zinc ions in early development.

Submission information

The zinc transporter, *Slc39a10/Zip10*, is required for the zinc sparks of fertilization in mice.

Introduction

In mammalian fertilization, the sperm factor is released into the ooplasm to activate the oocyte (Yoon and Fissore, 2007). It is now believed that phospholipase C zeta (PLCζ) (Yoon and Fissore, 2007; Saunders et al., 2002) is the sperm factor and its induces in the ooplasm repetitive increases in the

intracellular Ca^{2+}, termed 'calcium oscillations.' These oscillations play an essential role in triggering the oocyte activation events, such as cortical granule exocytosis, the block of polyspermy, meiotic resumption and exit from MII arrest (Xu et al., 1994; Jones, 2005; Ducibella et al., 2006; Ito et al., 2011; Sugita et al., 2024). A calcium increase is highly conserved in many species as the trigger of egg activation and is vital for successful fertilization.

In recent years, zinc ions as well as calcium ions, are thought to play important roles during fertilization (Suzuki et al., 2010; Allouche-Fitoussi and Breitbart, 2020; Kageyama et al., 2022). Zinc ion is an essential trace element and the second most abundant transition ion in the human body after iron (Lubna and Ahmad, 2023). Zinc homeostasis is essential for optimal metabolic function in the reproductive process in mammals (Pascua et al, 2020), therefore zinc deficiency causes abnormalities such as fetal teratogenicity, long gestation periods, problematic labor, low birth weight and weak offspring (Favier, 1992; Bedwal and Bahuguna, 1994). Zinc also has important role in the male and female germ cells (Allouche-Fitoussi and Breitbart, 2020; Kageyama et al., 2022). Especially in the mouse female germ cells, zinc-deficient condition caused profound defects in oocyte maturation, cumulus cell expansion and ovulation cycle (Tian and Diaz, 2012). Several studies have been conducted in mice to understand how zinc regulates oocyte maturation. Zinc was reported to be a critical regulator of meiosis throughout oocyte maturation, including maintaining release from the first and second meiotic arrest (Kong et al., 2012). In addition, zinc levels of oocytes were found to increase by 50% as the oocyte progressed through meiosis (Kim et al., 2010; Bernhardt et al., 2011).

In 2011, Kim *et al*. reported the importance of zinc during mammalian fertilization (Kim et al., 2011). Zinc is predominantly stored in vesicles that are symmetrically arranged along the oocyte cortex at the GV stage, and zinc-stored vesicles (cortical granules) are located away from the spindle and form a hemispherical pattern at the MII stage (Kim et al., 2011; Que et al., 2015; Kong et al., 2014; Que et al., 2019; Jo et al., 2019; Que et al., 2017). After the penetration of sperm, it has been induced a ‘zinc spark’ that releases billions of labile zinc ions from the cortical granules, and the total zinc content of the oocytes

101 decreases by 10-20% in at the end of fertilization in mice (Kim et al., 2011; Lee
102 et al., 2020). In addition, these events immediately follow a series of calcium
103 oscillations (Kim et al., 2011). Zinc spark has also been observed in the cattle,
104 non-human primate, human and Xenopus laevis oocytes (Kim et al., 2011; Que
105 et al., 2019; Duncan et al., 2016; Seeler et al., 2021), suggesting that this
106 phenomenon is a highly conserved event in vertebrate. More surprisingly, full-
107 term development of mouse embryos has been reported by chelation of Zn^{2+} ions
108 without Ca^{2+} release, suggesting the depletion of zinc ions in oocytes may be
109 sufficient for oocyte activation(Suzuki et al, 2010). Zinc has also been reported to
110 impact the sperm during fertilization in mice. Zinc accumulation in the zona
111 pellucida increases fibril binding along the glycoprotein matrix and decreases the
112 number of sperm that can reach the fertilized oocytes (Que et al., 2017; Aonuma
113 et al., 1981; Tokuhiro and Dean, 2018). After the zinc sparks, the released zinc
114 affects the forward motility of sperm to prevent their passage through the zona
115 matrix (Tokuhiro and Dean, 2018). Zinc spark is associated with the release of
116 ovastacin (*Astl*, the official gene name), which is required for the zona reaction,
117 and functions as a polyspermy block mechanism that is initiated only a few
118 minutes after fertilization (Tokuhiro and Dean, 2018).
119 The transport of zinc ions into and out of cells is regulated by zinc
120 transporters. In mammals, 14 zinc ion importers, called as ZIP (ZIP1-ZIP14),
121 have been identified (Fukada and Kambe, 2011; Takagishi et al., 2017; Kambe
122 et al., 2015). Previous study showed that mammalian oocytes regulate zinc
123 uptake through two maternally derived and cortically distributed zinc transporters,
124 ZIP6 and ZIP10 (Kong et al., 2014). Further, they reported that targeted disruption
125 using *Zip6*- and *Zip10*- specific morpholino injection or antibody incubation
126 induced alteration of the intracellular labile zinc content, spontaneous resumption
127 of meiosis from the PI arrest and premature arrest at a telophase I-like state
128 (Kong et al., 2014). It is clear from these reports that ZIP6 and ZIP10 are involved
129 in zinc transport in oocytes, but the mechanisms are not clear. ZIP6 and ZIP10
130 form and function in a complex (Taylor et al., 2016), regulate glycogen synthase
131 kinase (GSK-3) and other enzymes in breast and kidney cancer cells, and
132 regulate epithelial-mesenchymal transition (EMT) (Taylor et al., 2016; Pal et al.,

133 2014). ZIP10 is also involved in many life phenomena such as hair follicles, skin
134 epidermis and atopic dermatitis (Bin et al., 2017; Nakajima et al., 2020). In
135 addition, ZIP10 is also an essential gene for embryonic hematopoiesis (He et al.,
136 2023).
137 However, while functional analysis of the zinc transporters in various cells and
138 tissues has been conducted, the function of these zinc transporters in oocytes
139 has not been elucidated.
140 In this study, we generated oocyte specific *Zip6* and *Zip10* conditional
141 knockout mice and examined the function of ZIP10 in the oocytes and the
142 importance of zinc homeostasis during fertilization and embryonic development.
143 This study provides clues that elucidate its role in fertilization and embryonic
144 development, which is still largely unknown. In addition, this is the first report
145 confirming the function of the zinc transporter in oocytes, which will contribute to
146 future research.
147
148 **Results**
149 **Zinc transporters, ZIP6, and ZIP10, are expressed in mouse oocytes**
150 **through follicular development**
151 First, using *in situ* hybridization and immunofluorescent staining, we
152 examined the expression of ZIP10 during follicular development. As shown in Fig.
153 1A, *Zip10* mRNA was expressed from the primordial oocyte (Arrow). It continued
154 to be expressed in oocytes of primary, secondary, and antral follicles. ZIP10
155 protein was also expressed in the plasma membrane of primordial oocytes
156 (Fig.1B; Arrow). We also confirmed the expression of ZIP10 protein at the plasma
157 membrane of oocytes of primary, secondary, and antral follicles. Although ZIP6
158 was also expressed in oocytes throughout folliculogenesis (Fig.1C; Arrow), it
159 displayed nuclear localization in oocytes and granulosa cells of primary,
160 secondary, and antral follicles. Fig. 1D showed zona pellucida and granulosa
161 cells through the follicular development.
162
163 **Phenotype of oocyte-specific *Zip6*$^{d/d}$ and *Zip10*$^{d/d}$ female mice.**
164 To elucidate the roles of *Zip6* and *Zip10* in the mouse oocytes, oocyte-

165 specific *Zip6* (*Zip6*$^{d/d}$) and *Zip10* (*Zip10*$^{d/d}$) knockout mice were generated (Fig.
166 S1A-C). We examined whether ZIP6 and ZIP10 protein expression was absent
167 in *Zip6*$^{d/d}$ and *Zip10*$^{d/d}$ oocytes (Fig. S1D). *Zip6*$^{f/f}$ and *Zip10*$^{f/f}$ mice were used as
168 controls, respectively. We examined the number of ovulated oocytes or defects
169 in oocyte maturation. After superovulation, the number of ovulated oocytes
170 collected from the oviduct in *Zip10*$^{d/d}$ mice was 22.1 ± 2.5 oocytes/mouse (Fig.
171 2A), which was equivalent to that in *Zip10*$^{f/f}$ mice (18.7 ± 2.9 oocytes/mouse, $p >$
172 0.05). The numbers of ovulated oocytes in *Zip6*$^{d/d}$ and *Zip6*$^{f/f}$ mice were also
173 equivalent (28.7 ± 3.6 and 32.8 ± 3.3 oocytes/mice, respectively, $p > 0.05$) (Fig.
174 S2A). As for oocyte maturation, the rate of oocytes with a first polar body at 10h,
175 12h, and 14h in the *Zip10*$^{d/d}$ group was not different than that of *Zip10*$^{f/f}$ group
176 (*Zip10*$^{d/d}$: 58.7%, 61.9%, and 79.4%, *Zip10*$^{f/f}$: 50.8%, 54.1% and 70.5%,
177 respectively, $p > 0.05$, Fig. 2B). In addition, *Zip10*$^{d/d}$ oocytes display intact
178 metaphase spindles just as in the *Zip10*$^{f/f}$ groups (Fig. 2C).
179 Next, we examined the levels of labile zinc in germinal vesicle (GV), MII,
180 and two pronuclei (2PN) zygotes by comparing the fluorescence intensity
181 following loading with the dye, FluoZin-3AM (Fig. 2D). The FluoZin-3AM
182 fluorescence intensity in GV and MII oocytes of the *Zip10*$^{d/d}$ group was lower than
183 the *Zip10*$^{f/f}$ group ($p < 0.05$). After fertilization, the fluorescence intensity in *Zip10*$^{f/f}$
184 zygotes decreased dramatically, and also decreased for the *Zip10*$^{d/d}$ group,
185 although it remained higher than for *Zip10*$^{f/f}$ oocytes. When compared within
186 group, the fluorescence intensity in *Zip10*$^{f/f}$ between GV and MII oocytes was
187 significantly different (GV vs. MII and MII vs 2PN; $p < 0.05$, respectively), but the
188 stages of *Zip10*$^{d/d}$ oocytes were not different despite clear trends ($p > 0.05$). The
189 levels of zinc fluorescence intensity in the *Zip6*$^{d/d}$ group were not different from
190 the controls *Zip6*$^{f/f}$, which decreased markedly at fertilization (Fig. S2B; $p > 0.05$).
191

192 **The zinc sparks of *Zip10*$^{d/d}$ oocytes were suppressed after fertilization or**
193 **artificial activation.**

194 To determine if the absence of ZIP6 and ZIP10 influenced the detection of
195 Zn^{2+} sparks associated with fertilization, we monitored extracellular zinc and
196 intracellular calcium during fertilization of *Zip6*$^{d/d}$ and *Zip10*$^{d/d}$ oocytes (Fig. S3

197 and 3A). *Zip10*$^{f/f}$ oocytes displayed the expected calcium oscillations following
198 fertilization, and a zinc spark followed the first calcium rise (Fig. 3A upper side,
199 movies 1 and 2). In contrast, *Zip10*$^{d/d}$ oocytes did not release zinc ions
200 immediately after the first calcium spike, despite mounting normal calcium
201 oscillations (Fig. 3A lower side, movies 3 and 4). In *Zip6*$^{d/d}$ oocytes, a zinc spark
202 occurred immediately after the first intracellular calcium rise at fertilization, just as
203 in control *Zip6*$^{f/f}$ oocytes (Fig. S3, movie S1-S4). The extracellular zinc sparks
204 were examined following artificial oocyte activation of mouse oocytes with
205 ionomycin. The zinc sparks occurred immediately after the intracellular calcium
206 rise in *Zip10*$^{f/f}$ oocytes (Fig. 3B upper side, movies 5 and 6), however, *Zip10*$^{d/d}$
207 oocytes did not release zinc ions after the calcium spike (Fig. 3B lower side,
208 movies 7 and 8).
209
210 ***Zip10*$^{d/d}$ mouse oocytes can be fertilized but not developed to the blastocyst.**
211 *Zip6*$^{d/d}$ and *Zip10*$^{d/d}$ oocytes then were used for IVF, and we examined the
212 rates of fertilization, polyspermy, and embryo development. Successful
213 fertilization was confirmed at 6 h after IVF by the presence of pronuclei (Fig. 4A
214 and B). *Zip10*$^{d/d}$ oocytes were fertilized at rates like those observed for control
215 oocytes (Fig. 4A). Consistent with this, the zona reaction triggered by fertilization
216 and examined using a ZP2 antibody was similar in *Zip10*$^{d/d}$ and *Zip10*$^{f/f}$ oocytes
217 (Fig. 4D). We also examined the localization of ovastacin, whose expression in
218 the cortex and loss post-fertilization was comparable between the two groups (Fig.
219 4E). As for the expression of JUNO, it had the same expression than between
220 null and control oocytes and the temporal dynamics of its disappearance from the
221 cortex after fertilization was similar for both *Zip10*$^{f/f}$ and *Zip10*$^{d/d}$ groups (Fig. 4F).
222 We next examined the development to the blastocyst stage, and whereas
223 *Zip10*$^{f/f}$ zygotes developed at the expected rates, approximately 78.9% (2 cell),
224 90.3 (4-8 cell) and 75.0% (blastocyst) , a smaller fraction of *Zip10*$^{d/d}$ zygotes did
225 37.2% (2 cell) and 38.3% (4-8 cell) and only 32.7% reached blastocyst stage (p
226 < 0.05; Fig. 4B). As shown in Fig. 4C, the total cell numbers of blastocysts were
227 also lower for *Zip10*$^{d/d}$ embryos (51.6 ± 2.1 cells) than for those of *Zip10*$^{f/f}$ ones
228 (72.7 ± 2.1 cells, $p < 0.05$). *Zip6*$^{d/d}$ oocytes did not display any alterations in the

229 rate of fertilization or development (Fig. S2C and D; $p > 0.05$).

230

231 **Discussion**

232 The zinc sparks associated with fertilization were first discovered in the
233 mouse. Similar observations followed in other mammalian species and
234 amphibians. However, the underlying mechanism(s) and biological role of zinc
235 sparks are not elucidated. In this study, we have examined the role of the zinc
236 transporters ZIP6 and ZIP10 using conditionally gene deficient mice, and queries
237 their contribution to the zinc sparks of fertilization.

238 First, we confirmed the expression of zinc transporter in mouse oocytes.
239 Our results are consistent with previous studies (Kong et al., 2014; Chen et al.,
240 2023). ZIPs, including ZIP6 and ZIP10, are transmembrane proteins (Eide, 2004;
241 Kambe et al., 2004; Lu and Fu, 2007; Schmitt-Ulms et al., 2009). In primordial
242 follicles, the ooplasmic staining of ZIP10 we anticipate correspond to ooplasmic
243 vesicular sites. ZIP10 expression shifted to the plasma membrane in primary and
244 antral follicle phase. A similar localization shift of ZIP10 to the oocyte surface was
245 reported during oocyte maturation, which is much later than reported here by.
246 Furthermore, in that study, ZIP10 was detected in the nuclear/nucleolar positions
247 of oocytes of all follicular stages (Chen et al., 2023), which we did not observe.
248 On the other hand, ZIP6 was expressed at the nuclear/nucleolar regions and in
249 granulosa cells. This localization of ZIP6 was consistent with that in a previous
250 study (Chen et al., 2023). However, our results failed to notice that ZIP6 shifts to
251 the at plasma membrane in antral follicle oocytes (Kong et al., 2014; Chen et al.,
252 2023). The results indicate that ZIP6 may be fulfilling a distinct function within the
253 oocytes compared to ZIP10.

254 To assess the role of these transporters in mice, we generated oocyte-
255 specific *Zip6 or Zip10* knockout mice (Fig. S1; $Zip6^{d/d}$ and $Zip10^{d/d}$, respectively).
256 Previous reports noted that the disruption of these transporters using specific
257 morpholinos or incubation in function-blocking antibodies induced the change of
258 intracellular labile zinc quota into mice oocytes (Kong et al., 2014). The amount
259 of labile zinc ions in those mouse oocytes was measured using Fluozin-3AM, zinc
260 indicator. The amount of labile zinc ions in $Zip10^{d/d}$ oocytes was significantly lower

261 than in the *Zip10*$^{f/f}$ (Fig. 2D). We failed to observe any effect on zinc levels of in
262 *Zip6*$^{d/d}$ oocytes (Fig. S2B). The results indicate that ZIP10 is mostly responsible
263 for the uptake of zinc ions in mouse oocytes.

264 Zinc insufficient GV oocytes do not maintain the meiotic arrest at PI. This
265 is suggested to happen by premature activation of the MOS-MAPK pathway in
266 the presence of low zinc (Kong et al., 2012). In addition, low ooplasmic zinc
267 accelerates meiotic progression that contributes to the extrusion of large polar
268 bodies (Bernhard et al., 2011). The early mitotic inhibitor 2 (EMI2), a zinc-binding
269 APC/C proteasome inhibitor, is also an essential component of the cytoplasmic
270 factor (CSF) that initiates entry into MII phase. EMI2 is a zinc binding protein, and
271 when zinc is reduced, the activity of the APC/C proteasome is stimulated,
272 increasing the degradation of CCNB1, reduced MPF activity leading to early
273 release of meiosis arrest (Bernhardt et al., 2011; Bernhardt et al., 2012; Suzuki
274 et al., 2010, Shoji et al., 2014; Ohe et al., 2010). Previous studies reported that
275 targeted disruption of *Zip10* using morpholino injections and function-inhibiting
276 antibodies during meiotic maturation perturbed meiosis progression and resulted
277 in cell cycle arrest at the telophase I-like state (Kong et al., 2014). Based on these
278 findings we hypothesized that the reduced state of labile zinc ions in *Zip10*$^{d/d}$
279 mouse oocytes may resemble the state of zinc-deficient oocytes. We investigated
280 the maturation progression and spindle organization in oocyte matured in vitro
281 from the GV to MII stage. We failed to observe any differences (Fig. 2A, B and
282 C). We also did not observed abnormalities in oocytes from *Zip6*$^{f/f}$ mice (Fig. S2A;
283 $p > 0.05$). We speculate that the disparate outcomes observed in previous studies
284 may be attributed to the presence of trace amounts of labile zinc ions in media or
285 in the oocytes.

286 Surprisingly, the amount of labile zinc ions in *Zip10*$^{d/d}$ 2PN zygote was
287 higher than in *Zip10*$^{f/f}$ and despite some differences in fluorescence intensity
288 between *Zip10*$^{d/d}$ GV, MII and 2PN zygote, the labile zinc concentrations were
289 not significantly different between these groups (Fig. 2D). Therefore, we
290 monitored zinc sparks and calcium oscillations in the *Zip10*-KO oocytes. Several
291 studies reported the important of IP_3Rs in mammalian oocytes (Fissore et al.,
292 1999; Parrington et al., 1998), which is essential for egg activation because its

293 inhibition precludes Ca^{2+} oscillations (Miyazaki and Ito, 2006; Miyazaki et al.,
294 1992; Xu et al., 2003). It has been reported that a putative Zinc-finger motif in a
295 helical linker (LNK) domain near the C-terminus of *IP_3R1* plays a role in *IP_3R1*
296 function (Fan et al., 2015; Paknejad and Hite, 2018), Recently, Akizawa *et al*.,
297 reported that both deficient and excessive zinc ions compromise *IP_3R1* sensitivity,
298 diminishing and terminating calcium oscillations (Akizawa et al., 2023). Our
299 results showed that a single zinc spark occurs immediately after first calcium rise
300 of oscillations in *$Zip10^{f/f}$* oocytes, as reported by Kim *et al* (Kim et al., 2011) (Fig.
301 3A), and similar results are obtained in *$Zip6^{d/d}$* and *$Zip6^{f/f}$* mouse oocytes (Fig.
302 S3). However, in *$Zip10^{d/d}$* oocytes, despite the presence calcium elevations, zinc
303 sparks failed to occur. Similarly, *$Zip10^{d/d}$* oocytes activated with ionomycin
304 (artificial oocyte activation) did not show a zinc spark (Fig. 3B). In this study,
305 calcium oscillations occurred in oocytes with low zinc state. In addition, there was
306 no difference in the amplitude frequency of calcium ions in oocytes of both groups
307 within the observation time. Akizawa *et al*., produced zinc deficiency state with
308 TPEN, a strong chelator of intracellular labile zinc ions (Akizawa et al., 2023). On
309 the other hand, we did not completely remove intracellular labile zinc ions from
310 mouse oocytes. We speculate that zinc ions existed in *$Zip10^{d/d}$* mouse oocytes
311 induce Ca^{2+} release without compromising *IP_3R1* sensitivity. However, this study
312 demonstrated that the accumulation of intracellular zinc ions mediated by ZIP10
313 is essential for inducing zinc sparks in mouse oocytes.

314 The total cellular zinc ions content required for meiosis in the oocyte
315 substantially increases (a 50% increase) from the prophase I arrest to the arrest
316 at metaphase of meiosis II (Kim et al., 2010; Bernhardt et al., 2011). The zinc is
317 stored in undefined cortical granules, and an average of 10^6 zinc atoms are
318 released from these vesicles at the time of fertilization (exocytosis) (Kim et al.,
319 2011; Que et al., 2015; Kong et al., 2014; Que et al., 2019; Jo et al., 2019; Lee
320 et al., 2020). There are several possibilities that might explain why *Zip10*
321 conditional KO mice have low zinc sparks. The most logical is that these oocytes
322 experience reduced zinc loading of cortical of zinc vesicles, leading to the
323 absence of sparks. Our results suggest that in oocytes, zinc sparks and
324 exocytosis require adequate concentrations of labile zinc ions in the cortical

325 secretory vesicles, which is not accomplished when ZIP10 is not present.

326 Zinc sparks have been reported to contribute to the rapid and permanent
327 block mechanisms to prevent polyspermy. The former is achieved by zinc in the
328 extracellular milieu decelerating the forward motility of sperm (Tokuhiro and Dean,
329 2018). Secondly, the release of labile pools of zinc at the same time that the zinc
330 metalloendopeptidase ovastacin is released with the cortical granules (Tokuhiro
331 and Dean, 2018; Burkart et al., 2012; Schmitz et al., 2021), cause ZP2 protein
332 cleavage inducing a complete, although belated block to polyspermy (Que et al.,
333 2017; Aonuma et al., 1981; Tokuhiro and Dean, 2018). However, the
334 physiological significance of the zinc sparks' contributions to polyspermy have
335 not been thoroughly tested, and *Zip10*$^{d/d}$ mice, which are almost devoid of them,
336 offer a great model. Our results showing normal rates of monospermic fertilization
337 in *Zip10*$^{d/d}$ *oocyte* suggest that contributions of Zinc to polyspermy control is
338 negligible (Fig. 4A). Our results also show that the ovastacin undergoes normal
339 release in *Zip10*$^{f/f}$ oocytes after fertilization (Fig. 4E and 4D), confirming previous
340 studies of a minor role of the ZP2 to polyspermy. We observed the disappearance
341 of JUNO after fertilization (Bianchi et al., 2014) *Zip10*$^{d/d}$*,* suggesting that gamete
342 fusion took place (Fig. 4F). Together, these results support the view that zinc
343 spark is not directly involved in the polyspermy rejection mechanism.

344 Interestingly, there were no differences in the rates of fertilization
345 (pronucleus formation), but development to the blastocyst stage was significantly
346 reduced in *Zip10*-null embryos (Fig. 4B). Most of the embryos were arrested at
347 the 2-cell stage and not developed beyond the 4-cell stage. Zinc insufficiency
348 caused altered chromatin structure in the nuclei of blastomeres that displayed
349 decreased global transcription, causing arrest in embryonic development (Kong
350 et al., 2015). The abnormal zinc homeostasis, particularly during the one-cell
351 stage, inhibits the activation of the embryonic genome that occurs around the
352 two-cell stage in mice due to reduce the translational capacity through the
353 inhibition of ribosomal RNA synthesis by RNA polymerase I (Chanfreau, 2013;
354 Garner et al., 2021). Our results also show that *Zip10*$^{d/d}$ blastocysts had
355 significantly lower cell numbers compared to the blastocysts from *Zip10*$^{f/f}$ mice
356 (Fig. 4C). Our results suggest that Zip10$^{d/d}$ mice oocytes can be fertilizable, but

357 their developmental potential is decreased. The lack of ZIP10-mediated zinc
358 influx during the folliculogenesis of *Zip10*$^{d/d}$ may compromise gene expression
359 during these early stages of oocyte development. *Zip10*$^{d/d}$ mouse oocytes thus
360 may have compromised developmental potential from the outset. Future studies
361 should assess the transcriptomic profile of *Zip10*$^{d/d}$ mouse oocytes.
362 In conclusion, we elucidated that ZIP10 is required for zinc ion uptake into
363 oocytes and the intracellular zinc ions regulated by ZIP10 was important for zinc
364 sparks and progression of embryonic development. Currently, the many infertility
365 patients exist in the world (the survey of WHO). It is reported that approximately
366 half of the adult females are deficient in zinc in their serum (Prasad, 1996;
367 Yokokawa et al., 2020). Zinc has been reported to play essential roles in many
368 physiological functions including reproductive functions. The findings will help
369 elucidate the role of zinc homeostasis in the fields of fertilization/embryogenesis.
370 Furthermore, the development of zinc-focused assisted reproductive
371 technologies and fertilization/embryogenesis media could contribute to improve
372 the developmental potential of oocytes and embryos in other mammalian species.
373

374 **Materials and Methods**

375 All chemicals and reagents were purchased from Sigma-Aldrich (St. Louis, MO,
376 USA) unless otherwise stated.
377

378 **Animals**

379 Animals were housed in the barrier facility at Azabu University. The
380 deletion of the ZIP10 gene in the whole body is known to result in embryonic
381 lethality (He et al., 2023). The conditional knockout mice were generated by Cre-
382 loxP system. The following mouse strains were used: *Zip10*$^{flox/flox}$ (*Zip10*$^{f/f}$) mouse
383 <B6;129-Slc39a10 <tm1.1Tfk>> (RBRC06221) (Hojyo et al., 2014; Miyai et al.,
384 2014; Bin et al., 2017) was provided by the RIKEN BRC through the National
385 BioResource Project of the MEXT/AMED, Japan. *Zip6*$^{flox/flox}$ (*Zip6*$^{f/f}$) mouse
386 <B6;129-Slc39a6> was generated by AdAMS. *Gdf9*$^{Cre/+}$ mice <Stock Tg (GDF9-
387 iCre) 5092Coo/J, Stock No: 011062> were delivered from Jackson Laboratory
388 (Lan et al., 2004). Crlj: C57BL/6J female mice (6-8 weeks old) and Crlj: C57BL/6J

389 male mice (8-12 weeks old) were purchased from Charles River Laboratories
390 Japan (Yokohama, Japan). The mice were housed under controlled lighting
391 conditions (daily light period, 0600-1800 h). The study was approved by the
392 Animal Experimentation Committees of Azabu University and were performed in
393 accordance with the committees' guidelines (200318-13 and 230309-1). Oocyte-
394 specific gene knockout (*Zip10*$^{f/f}$, *Gdf9*$^{Cre/+}$; *Zip10*$^{d/d}$) mice were generated by
395 crossing *Gdf9*$^{Cre/+}$ male mice with *Zip10*$^{f/f}$ female mice (Fig. S1A-E). Similarly,
396 *Zip6*$^{d/d}$ mice were generated (Fig. S1A-E).
397
398 **In situ hybridization (ISH)**
399 ISH was performed as previously described with some modifications
400 (Namiki et al., 2023). Briefly, fixed ovaries were paraffin-embedded and paraffin
401 sections (6 μm) were mounted on MAS-coated slides (Matsunami Glass
402 Industries, Osaka, Japan) under RNase-free conditions. Sense or antisense
403 digoxigenin (DIG)-labeled RNA probes for *Slc39a10* (*Zip10*) were purchased
404 from Genostaff. The sections were deparaffinized, rehydrated, and post-fixed in
405 10% neutral buffered formalin (NBF) for 30 min at 37°C, followed by the treatment
406 with 0.2% hydrogen chloride and 5 μg/ml proteinase K (FUJIFILM Wako Pure
407 Chemical, Osaka, Japan) for 10 min at 37°C, respectively. Hybridization was
408 performed with DIG-labeled probes (250 ng/ml) in a humidified chamber at 60°C
409 overnight. The slides were washed after hybridization, then treated with blocking
410 reagent (Genostaff) for 15 min and alkaline phosphatase-conjugated anti-DIG
411 antibody (1:2,000; Roche Diagnostics, Basel, Switzerland) for 1 h at room
412 temperature. The signals were detected by 4-nitro-blue tetrazolium/5-bromo-4-
413 chloro-3-indolyl phosphate (NBT/BCIP, Roche Diagnostics) in a humidified
414 container for 12 h at 4°C. The sections were counterstained with Kernechtrot
415 solution (Muto Pure Chemicals, Tokyo, Japan). Signals detected by the sense
416 probe were used as a control for background levels.
417
418 **Immunofluorescent staining (IF) for ovary**
419 IF was performed as previously described with some modifications
420 (Namiki et al., 2023). Fixed ovaries were paraffin-embedded and the sections (6

421 μm) were deparaffinized, hydrated and conducted for antigen retrieval by
422 autoclaving in 10 mM sodium citrate buffer (pH = 6.0) for 5 min. The sections
423 were further incubated on ice for 30 min. After blocking with Bloking One Histo
424 (06349-64, NACALAI TESQUE Inc, Kyoto, Japan) for 1 h, the slides were
425 incubated with primary antibody for Rabbit anti-mouse-Zip10 (1:200; (Miyai et al.,
426 2014)), Rabbit anti-SLC39A6 (1:200, HPA042377, Sigma), Rabbit anti-Foxl2
427 (1:300; (Cocquet et al., 2002; Polanco et al., 2010)), Rat anti-ZP2 (1:100, sc-
428 32752, Santa Crus Biotechnology, Dallas, Texas, USA) in Can Get Signal
429 immunostain (TOYOBO, Tokyo, Japan) overnight at 4°C. The slides were
430 incubated with Alexa Fluor 488 donkey anti-rabbit IgG (H+L), Alexa Fluor 594
431 donkey anti-rabbit IgG (H+L) or Alexa Fluor 488 donkey anti-rat IgG (H+L)
432 conjugated secondary antibodies (Jackson Immuno Research Laboratories,
433 West Grove, PA, USA) diluted 1:500 in Can Get Signal immunostain (TOYOBO)
434 for 1 h, and mounted with ProLong Glass Antifade Mountant with NucBlue Stain
435 (P36981, Thermo Fisher Scientific, Waltham, MA, USA). Micrographs were
436 captured by BZ-X700 microscopy (Keyence, Osaka, Japan).
437
438 **Oocyte preparation**
439 Germinal vesicle (GV) oocytes were collected in the manner described in
440 our previous study (Ito et al., 2008) with some modifications. Ovaries were
441 collected from female mice 48 h after intraperitoneally injection with 5 IU equine
442 chorionic gonadotropin (eCG) (PMS; Nippon Zenyaku Kogyo, Fukushima, Japan).
443 They were placed in a 35 mm culture dish containing MEMα (no nucleosides,
444 powder; Gibco/Thermo Fisher Scientific, Tokyo, Japan) medium with 26 mM
445 $NaHCO_3$, 75 mg/l penicillin, 50 mg/l streptomycin sulfate, 5% (v/v) heat-treated
446 fetal calf serum (FCS), and 10 ng/ml epidermal growth factor (EGF). Cumulus-
447 oocyte complexes (COCs) were released from the antral follicles by gentle
448 puncturing with a needle.
449 To obtain metaphase II (MII) oocytes, the mice were intraperitoneally
450 injected with 5 IU eCG followed by injection with 5 IU human chorionic
451 gonadotropin (hCG) (Gonatropin; ASKA Pharmaceutical, Tokyo, Japan) at 48 h
452 later. COCs were collected from the oviductal ampulla 14-16 h after hCG injection.

453 These oocytes were used in the following experiments.
454
455 **Count of ovulated oocytes**
456 COCs-MII were obtained by superovulation treatment. The cumulus cells
457 were removed from the COCs-MII with hyaluronidase (1 mg/ml) and gentle
458 pipetting. All collected oocytes were counted and calculated as the number of
459 ovulations.
460
461 **In vitro maturation (IVM) of GV oocytes**
462 IVM were conducted in the manner described in our previous study
463 (Kamoshita et al., 2021) with some modifications. Ovaries were placed in a 35
464 mm culture dish containing MEMα medium with 26 mM $NaHCO_3$, 75 mg/l
465 penicillin, 50 mg/l streptomycin sulfate, 5% (v/v) FCS, and 10 ng/ml EGF. COCs-
466 GV were released from the antral follicles by gentle puncturing with a needle. The
467 COCs-GV were washed 3 times and cultured in 500 µl of same medium in 4-well
468 dish at 37°C in an atmosphere of 5% CO_2 in air for 10, 12 and 14 h. After the
469 culture, cumulus cells were removed from the COCs with hyaluronidase (1 mg/ml)
470 and gentle pipetting. The extrusion of 1st polar body was evaluated at each time.
471
472 **IF for oocytes/preimplantation embryos**
473 The α-tubulin and JUNO (PE anti-mouse FR4) were performed with some
474 modification of the methods of Inoue *et al* (Inoue et al., 2017). The oocytes or
475 embryos were fixed in 4% PFA for 30 min at room temperature, washed in PBS
476 containing 1% polyvinyl alcohol (PBS/PVA). They were permeabilized by
477 treatment of 0.5% Triton X-100 for 15 min and washed 2 times in 1%
478 BSA/PBS/PVA followed by blocked for 20 min in same medium. They were
479 incubated for overnight at 4° with primary antibodies to rabbit anti-α-tubulin
480 (1:200; 11H10, cell Signaling Technology) or rat anti-mouse FR4 (JUNO; 1:250;
481 12A5 BioLegend), wash 3 times in 1% BSA/PBS/PVA. Primary antibodies were
482 detected using Alexa Fluor 488 donkey anti-rabbit IgG (H+L) (1:250) or Alexa
483 Fluor 488 donkey anti-rat IgG (H+L) (1:250) for 1 h at room temperature. After

484 staining, all samples mounted in VECTASHIELD Mounting Medium with DAPI (H-
485 1200; Vector Laboratories, California, USA), imaged using BZ-X700 microscopy
486 (Keyence, Osaka, Japan).
487 The ovastacin staining was performed with some modifications of the
488 methods of Burkart *et al* (Burkart et al., 2012). oocytes or embryos were fixed in
489 4% PFA for overnight at 4 ^{o}C, washed in PBS containing 0.3%
490 polyvinylpyrrolidone (PVP), and then blocked in 0.3% BSA/0.1 M glycine (three
491 times for 10 min) followed by permeabilization in 0.2% Triton X-100 for 15 min
492 (Baibakov et al., 2007). Samples were then incubated for overnight at 4°C with
493 Rabbit polyclonal anti-ovastacin (Burkart et al., 2012), 1:200, gifted antibody),
494 washed with 0.3% PVP/0.1% Tween (three times for 10 min), and incubated for
495 1 h at room temperature with Alexa Fluor 488 anti-rabbit secondary antibody
496 (1:500) followed by staining and mounting with VECTASHIELD Mounting Medium
497 with DAPI. Samples were imaged using TCS SP5 II confocal microscope (Leica
498 Microsystems, Wetzlar, Germany).
499
500 **In vitro fertilization (IVF)**
501 IVF and sperm collection were conducted with some modification of the
502 method described in our previous study (Kageyama et al., 2023). In brief,
503 ovulated COCs-MII were preincubated for 1 h in 80 μl human tubal fluid (HTF)
504 droplets supplemented with 1.25 mM reduced glutathione (GSH). Frozen-thawed
505 sperm suspensions were suspended in 200 μl preincubation medium (HTF
506 containing 0.4 mM methyl-β-cyclodextrin) and 0.1 mg/ml PVA, but without bovine
507 serum albumin, and were incubated at 37 ^{o}C under 5% CO_2 in humidified air for
508 1 h. At the time of insemination, preincubated spermatozoa were transferred into
509 the droplets with oocytes at final concentrations of 2.0×10^{6} sperm/ml. After 6 h,
510 oocytes were separated from spermatozoa and cumulus cells using a fine glass
511 pipette and transferred into 50 μl KSOMaa medium. They were cultured at 37 ^{o}C
512 under 5% CO_2 in humidified air for approximately 24-96 h. The embryos were
513 observed at 24, 48, 72, and 96h after IVF, and the number of 2cell, 4-8cell, morula,
514 and blastocyst stage embryos were counted, respectively. The oocytes used for
515 IVF were calculated as the parameter for the fertilization rate and the rate of

516 embryo development. After IVF at 96 h, the blastocysts were fixed in 4% PFA for
517 30 min at room temperature. Following three times washed in PBS/PVA for 30
518 min each. Nuclear DNA was stained and mounted in VECTASHIELD Mounting
519 Medium with DAPI. Cell numbers were determined by visually inspecting nuclei
520 stained with DAPI using an inverted fluorescence microscope.
521
522 **Zinc measurements**
523 FluoZin-3AM staining was conducted using the method described in our
524 previous study (Kageyama et al., 2022). The obtained GV oocytes, cumulus cells
525 were removed from the COCs with gentle pipetting. The obtained MII oocytes,
526 cumulus cells were removed from the COCs with hyaluronidase (1 mg/ml) and
527 gentle pipetting. Oocytes with a polar body were defined as MII. After IVF for 6h,
528 two pronucleus stage embryos (2PN) were collected. GV, MII and 2PN were
529 loaded in 50 μl medium that was suitable for each stage containing the amyl ester
530 of the membrane permeant zinc-specific fluorophore, FluoZin-3AM (2 μM;
531 F24195, Thermo Fisher Scientific, excitation 494 nm/emission 516 nm) for 1 h in
532 humidified CO_2 [5% (v/v) in air] at 37 ^{o}C followed by washing three times in
533 medium and then observation with TCS SP5 II confocal microscope. FluoZin-3
534 has been extensively characterized for measurements of free intracellular zinc in
535 live cells using microscopy and has an affinity constant (Kd) for zinc of 15 nM
536 (Gee et al., 2002a; Gee et al., 2002b). Our previous study showed MII oocytes
537 were treated with FluoZin-3 AM for 60 min, the change of fluorescence was
538 confirmed in the cytoplasm of the oocytes and embryos, suggesting this treatment
539 duration with FluoZin-3 AM is suitable for detection of zinc ions in oocytes and
540 embryos(Kageyama et al., 2022). The pixel intensity per unit area after
541 background subtraction was determined in GV, MII and 2PN within the circle
542 (white circle) and ImageJ image processing software.
543
544 **Measurement of Ca^{2+} and Zinc spark during fertilization**
545 Fresh or frozen-thawed sperm suspension were suspended in 200 μl
546 preincubation medium. The 1 μl (fresh) or 20 μl (frozen-thawed) sperm
547 suspension were placed in 40-80 μl HTF drop in pre-insemination dish about 20

548 min before insemination. The zona pellucida were punctured by piezo-electric
549 pulses applied to four locations with a 15 μm injection needle. The treated MII
550 oocytes were cultured in CZB containing CalbryteTM 590 AM (10 μM, #20700,
551 AAT Bioquest, CA, USA, excitation 581 nm/emission 593 nm) for 10 min in
552 humidified CO_2 [5% (v/v) in air] at 37 °C. While the oocytes are incubated for 10
553 min, make a drop of 10 μl of PVA(-), Ca(-) Hepes-CZB (H-CZB) and pull out 7 μl
554 of medium from drop with pipette man in the insemination dish. After 10 min, the
555 oocytes are washed and transferred to insemination dish and the oocytes are
556 attached to the dish. After attachment, an HTF containing 7 μl of BSA and a
557 membrane-impermeable zinc-specific fluorophore, FluoZin-3 (20 μM, F24194,
558 Thermo Fisher Scientific, excitation 494 nm/emission 516 nm), is added to the 3
559 μl drop containing the oocytes gently using a capillary. The about 1 μl sperm were
560 sucked from the pre-insemination drop with the capillary under a
561 stereomicroscope and place into the drop containing the oocytes, to start imaging.
562 In case ionomycin treatment, after calcium labeling, MII were allowed to settle in
563 45 μl PVA(-), Ca(-) H-CZB containing FluoZin-3 medium drop on dish, to start
564 imaging. The 5 μl ionomycin (5 μM; #407950) were added to MII at 2 min after
565 imaging start. Imaging was performed on confocal microscope using 488 nm
566 (Zn^{2+}) and 555 nm (Ca^{2+}) excitation (Nikon solutions, Tokyo, Japan) for max 50
567 min every 4 seconds. Imaging analysis was performed by defining regions of
568 interest (ROIs) and measuring fluorescence intensity over time using NIS-
569 Elements (Nikon). The intracellular ROIs were drawn as the entire interior area
570 of the cell. The extracellular ROIs were defined as a ring around the perimeter of
571 cell. The ring thickness was conserved for all data analyses.
572
573 **Western blotting**
574 Western blotting was carried out as described (Ito et al., 2010) with some
575 modifications. Thirty MII oocytes or 2PN embryos were lysed in Laemmli sample
576 buffer (Bio-Rad Laboratories, Tokyo, Japan) with 5% 2-mercaptoethanol.
577 Samples were separated on 8% Bis-Tris gels by SDS-PAGE and transferred to
578 PVDF membranes (Bio-Rad). The PVDF membranes were blocked in 10% skim
579 milk (FUJIFILM Wako) in Tris-buffered saline (TBS) with 0.1% Tween-20

580 (Yoneyama yakuhin kogyo, Osaka, Japan) and probed with primary antibody to
581 Rabbit anti-mouse-Zip10 (1:1,000; (Miyai et al., 2014)), Rabbit anti-SLC39A6
582 (1:1,000, HPA042377), rat anti-ZP2 (1:1,000) or monoclonal mouse anti-β-actin
583 (1:5,000; A5316, Sigma-Aldrich) for overnight at 4°C. The membranes were
584 incubated with secondary antibody; HRP-conjugated anti-rabbit IgG (1:5,000;
585 Cell Signaling Technology, Danvers, MA, USA), HRP-conjugated anti-rat IgG
586 (1:5000; Cell Signaling Technology) or HRP-conjugated anti-mouse IgG (1:5,000;
587 Cell Signaling Technology) for 1 h at room temperature. After washing of the
588 membranes, immunoreactive proteins were visualized using ECL™ Western
589 Blotting Analysis System (Cytiva Global Life Sciences Technologies, Tokyo,
590 Japan), according to the manufacture's recommendation. The membranes were
591 exposed by ImageQuant LAS 4000. After exposure, the membranes were
592 incubated for 30 min at 50 °C in the stripping buffer including 1.5 M Tris-HCl (pH
593 6.8), 10% SDS, 2-mercaptoethanol followed by extensive washing of the
594 membranes. The membranes were probed with primary antibody to mouse anti-
595 β-actin (1:5000; Sigma-Aldrich) for overnight at 4°C. The membranes were
596 incubated with secondary antibody; FRP-conjugated anti-mouse IgG (1:5000;
597 Cell Signaling) for 1 h at room temperature. The same procedure was followed
598 below.
599
600 **Statistical analysis**
601 Values from three or more times were used for evaluation of statistical
602 significance. Statistical analysis was performed using Statcel 3 software (OMS
603 Ltd., Saitama, Japan). The fertility, the total numbers of oocytes collected from
604 each mouse, the percentage of first polar extrusions, the fluorescence intensity
605 of Fluozin-3 AM and the cell count of blastocysts were evaluated statistically by
606 Student's t-test analysis. The rate of fertilization and embryo development was
607 analyzed using chi square tests. Values are shown as means ± S.E.M, and
608 significant differences were considered at p values < 0.05.
609
610
611 **Acknowledgments and funding sources**

We thank the members of the Laboratory of Animal Reproduction, School of Veterinary Medicine, Azabu University for technical help. *Zip10*$^{flox/flox}$ (*Zip10*$^{f/f}$) mouse <B6;129-Slc39a10 <tm1.1Tfk>> (RBRC06221) was provided by the RIKEN BRC through the National BioResource Project of the MEXT/AMED, Japan. We also thank Dr. Austin J. Cooney (The University of Texas at Austin, Austin, United States) for providing GDF9-iCre mice. This research was supported by Grants-in-Aid for Scientific Research from the Japan Society for the Promotion of Science (JSPS) (KAKENHI, 21H02384 and 20H05373 to J.I., 22H04268, 24H02601 and 24K23214 to A.K.), JSPS KAKENHI Grant Number JP 15H04584 (AdAMS) to JI, the Sasakawa Scientific Research Grant from The Japan Science Society (2019-4044) to A.K. and Mishima Kaiun Memorial Foundation (A-135) to A.K. This work was supported by JSPS KAKENHI Grant Number JP 22H04922 (AdAMS). This study was also supported by Center for Diversity, Equity & Inclusion, Azabu University (A.K). This research was partially supported by the Center for Human and Animal Symbiosis Science, Azabu University and a research project grant awarded by the Azabu University Research Services Division to J.I.

Author contributions

Conceptualization: A.K., J.I., Data curation: A.K., Methodology: N.O., T.W., A.O., Investigation: A.K., N.O., T.N., Y.K., Resources: M.O., Y.Y., T.F., Visualization: A.K., N.O., T.N., Supervision: A.O., T.F., R.A.F. J.I., N.K., Writing—original draft: A.K., Writing—review & editing: All the authors reviewed and edited the manuscript.

Competing interests

All other authors declare they have no competing interests.

Data and materials availability

All data are available in the main text or the supplementary materials.

References

Akizawa H, Lopes E, Fissore RA. 2023. Zn(2+) is Essential for Ca(2+) Oscillations in Mouse Eggs. *bioRxiv* doi:10.1101/2023.04.13.536745

Allouche-Fitoussi D, Breitbart H. 2020. The Role of Zinc in Male Fertility. *Int.J.Mol.Sci*. **21:**7796. doi: 10.3390/ijms21207796. doi:10.3390/ijms21207796

Aonuma S, Okabe M, Kawaguchi M, Kishi Y. 1981. Zinc effects on mouse spermatozoa and in-vitro fertilization. *J.Reprod.Fertil*. **63:**463–466. doi:10.1530/jrf.0.0630463

Baibakov B, Gauthier L, Talbot P, Rankin TL, Dean J. 2007. Sperm binding to the zona pellucida is not sufficient to induce acrosome exocytosis. *Development* **134:**933–943. doi:10.1242/dev.02752

Bedwal RS, Bahuguna A. 1994. Zinc, copper and selenium in reproduction. *Experientia* **50:**626–640. doi:10.1007/BF01952862

Bernhardt ML, Kim AM, O'Halloran TV, Woodruff TK. 2011. Zinc requirement during meiosis I-meiosis II transition in mouse oocytes is independent of the MOS-MAPK pathway. *Biol.Reprod*. **84:**526–536. doi:10.1095/biolreprod.110.086488

Bernhardt ML, Kong BY, Kim AM, O'Halloran TV, Woodruff TK. 2012. A zinc-dependent mechanism regulates meiotic progression in mammalian oocytes. *Biol.Reprod*. **86:**114. doi:10.1095/biolreprod.111.097253

Bianchi E, Doe B, Goulding D, Wright GJ. 2014. Juno is the egg Izumo receptor and is essential for mammalian fertilization. *Nature* **508:**483–487. doi:10.1038/nature13203

Bin B, Bhin J, Takaishi M, Toyoshima K, Kawamata S, Ito K, Hara T, Watanabe T, Irie T, Takagishi T, Lee S, Jung H, Rho S, Seo J, Choi D, Hwang D, Koseki H, Ohara O, Sano S, Tsuji T, Mishima K, Fukada T. 2017. Requirement of zinc transporter ZIP10 for epidermal development: Implication of the ZIP10-p63 axis in epithelial homeostasis. *Proc.Natl.Acad.Sci.U.S.A*. **114:**12243–12248. doi:10.1073/pnas.1710726114

Burkart AD, Xiong B, Baibakov B, Jimenez-Movilla M, Dean J. 2012. Ovastacin, a cortical granule protease, cleaves ZP2 in the zona pellucida to prevent polyspermy. *J.Cell Biol*. **197:**37–44. doi:10.1083/jcb.201112094

Chanfreau GF. 2013. Zinc'ing down RNA polymerase I. *Transcription* **4:**217–220. doi:10.4161/trns.26594

678 Chen Y, Chen S, Ok K, Duncan FE, O'Halloran TV, Woodruff TK. 2023. Zinc
679 dynamics regulate early ovarian follicle development. *J.Biol.Chem*. **299:**102731.
680 doi:10.1016/j.jbc.2022.102731

681 Cocquet J, Pailhoux E, Jaubert F, Servel N, Xia X, Pannetier M, De Baere E,
682 Messiaen L, Coti C, Fellous M, Veitia RA. 2002. Evolution and expression of
683 FOXL2. *J.Med.Genet*. **39:**916–921. doi:10.1136/jmg.39.12.916

684 Ducibella T, Schultz RM, Ozil J. 2006. Role of calcium signals in early
685 development. *Semin.Cell Dev.Biol*. **17:**324–332.
686 doi:10.1016/j.semcdb.2006.02.010

687 Duncan FE, Que EL, Zhang N, Feinberg EC, O'Halloran TV, Woodruff TK.
688 2016. The zinc spark is an inorganic signature of human egg activation.
689 *Sci.Rep*. **6:**24737. doi:10.1038/srep24737

690 Eide DJ. 2004. The SLC39 family of metal ion transporters. *Pflugers Arch*.
691 **447:**796–800. doi:10.1007/s00424-003-1074-3

692 Fan G, Baker ML, Wang Z, Baker MR, Sinyagovskiy PA, Chiu W, Ludtke SJ,
693 Serysheva II. 2015. Gating machinery of InsP3R channels revealed by electron
694 cryomicroscopy. *Nature* **527:**336–341. doi:10.1038/nature15249

695 Favier AE. 1992. The role of zinc in reproduction. Hormonal mechanisms.
696 *Biol.Trace Elem.Res*. **32:**363–382. doi:10.1007/BF02784623

697 Fissore RA, Longo FJ, Anderson E, Parys JB, Ducibella T. 1999. Differential
698 distribution of inositol trisphosphate receptor isoforms in mouse oocytes.
699 *Biol.Reprod*. **60:**49–57. doi:10.1095/biolreprod60.1.49

700 Fukada T, Kambe T. 2011. Molecular and genetic features of zinc transporters
701 in physiology and pathogenesis. *Metallomics* **3:**662–674.
702 doi:10.1039/c1mt00011j

703 Gee KR, Zhou ZL, Qian WJ, Kennedy R. 2002a. Detection and imaging of zinc
704 secretion from pancreatic beta-cells using a new fluorescent zinc indicator.
705 *J.Am.Chem.Soc*. **124:**776–778. doi:ja011774y [pii]

706 Gee KR, Zhou ZL, Ton-That D, Sensi SL, Weiss JH. 2002b. Measuring zinc in
707 living cells. A new generation of sensitive and selective fluorescent probes. *Cell*
708 *Calcium* **31:**245–251. doi:10.1016/S0143-4160(02)00053-2

709 He X, Ge C, Xia J, Xia Z, Zhao L, Huang S, Wang R, Pan J, Cheng T, Xu P,
710 Wang F, Min J. 2023. The Zinc Transporter SLC39A10 Plays an Essential Role
711 in Embryonic Hematopoiesis. *Adv.Sci.(Weinh)* **10:**e2205345.
712 doi:10.1002/advs.202205345

Hojyo S, Miyai T, Fujishiro H, Kawamura M, Yasuda T, Hijikata A, Bin B, Irie T, Tanaka J, Atsumi T, Murakami M, Nakayama M, Ohara O, Himeno S, Yoshida H, Koseki H, Ikawa T, Mishima K, Fukada T. 2014. Zinc transporter SLC39A10/ZIP10 controls humoral immunity by modulating B-cell receptor signal strength. *Proc.Natl.Acad.Sci.U.S.A*. **111:**11786–11791. doi:10.1073/pnas.1323557111

Inoue A, Jiang L, Lu F, Suzuki T, Zhang Y. 2017. Maternal H3K27me3 controls DNA methylation-independent imprinting. *Nature* **547:**419–424. doi:10.1038/nature23262

Ito J, Parrington J, Fissore RA. 2011. PLCzeta and its role as a trigger of development in vertebrates. *Mol.Reprod.Dev*. **78:**846–853. doi:10.1002/mrd.21359

Ito J, Yoon S, Lee B, Vanderheyden V, Vermassen E, Wojcikiewicz R, Alfandari D, De Smedt H, Parys JB, Fissore RA. 2008. Inositol 1,4,5-trisphosphate receptor 1, a widespread Ca2+ channel, is a novel substrate of polo-like kinase 1 in eggs. *Dev.Biol*. **320:**402–413. doi:10.1016/j.ydbio.2008.05.548

Ito J, Yoshida T, Kasai Y, Wakai T, Parys JB, Fissore RA, Kashiwazaki N. 2010. Phosphorylation of inositol 1,4,5-triphosphate receptor 1 during in vitro maturation of porcine oocytes. *Anim.Sci.J*. **81:**34–41. doi:10.1111/j.1740-0929.2009.00699.x

Jo Y, Lee I, Jung S, Kwon J, Kim N, Namgoong S. 2019. Spire localization via zinc finger-containing domain is crucial for the asymmetric division of mouse oocyte. *FASEB J*. **33:**4432–4447. doi:10.1096/fj.201801905R

Jones KT. 2005. Mammalian egg activation: from Ca2+ spiking to cell cycle progression. *Reproduction* **130:**813–823. doi:10.1530/rep.1.00710

Kageyama A, Terakawa J, Ito J, Kashiwazaki N. 2022. Roles of zinc signaling in mammalian reproduction. *Metallomics Research*. **2**

Kageyama A, Suyama A, Kinoshita R, Ito J, Kashiwazaki N. 2022. Dynamic changes of intracellular zinc ion level during maturation, fertilization, activation, and development in mouse oocytes. *Anim.Sci.J*. **93:**e13759. doi:10.1111/asj.13759

Kageyama A, Tsuchiya M, Terakawa J, Ito J, Kashiwazaki N. 2023. A combined treatment with progesterone, anti-inhibin serum, and equine chorionic gonadotropin improves number of ovulated oocytes in young C57BL/6J mice. *J.Reprod.Dev*. **69:**223–226. doi:10.1262/jrd.2023-036

748 Kambe T, Yamaguchi-Iwai Y, Sasaki R, Nagao M. 2004. Overview of
749 mammalian zinc transporters. *Cell Mol.Life Sci*. **61:**49–68. doi:10.1007/s00018-
750 003-3148-y

751 Kambe T, Tsuji T, Hashimoto A, Itsumura N. 2015. The Physiological,
752 Biochemical, and Molecular Roles of Zinc Transporters in Zinc Homeostasis
753 and Metabolism. *Physiol.Rev*. **95:**749–784. doi:10.1152/physrev.00035.2014

754 Kamoshita M, Fujiwara K, Ito J, Kashiwazaki N. 2021. Highly successful
755 production of viable mice derived from vitrified germinal vesicle oocytes. *PLoS*
756 *One* **16:**e0248050. doi:10.1371/journal.pone.0248050

757 Kim AM, Bernhardt ML, Kong BY, Ahn RW, Vogt S, Woodruff TK, O'Halloran
758 TV. 2011. Zinc sparks are triggered by fertilization and facilitate cell cycle
759 resumption in mammalian eggs. *ACS Chem.Biol*. **6:**716–723.
760 doi:10.1021/cb200084y

761 Kim AM, Vogt S, O'Halloran TV, Woodruff TK. 2010. Zinc availability regulates
762 exit from meiosis in maturing mammalian oocytes. *Nat.Chem.Biol*. **6:**674–681.
763 doi:10.1038/nchembio.419

764 Kong BY, Duncan FE, Que EL, Kim AM, O'Halloran TV, Woodruff TK. 2014.
765 Maternally-derived zinc transporters ZIP6 and ZIP10 drive the mammalian
766 oocyte-to-egg transition. *Mol.Hum.Reprod*. **20:**1077–1089.
767 doi:10.1093/molehr/gau066

768 Kong BY, Bernhardt ML, Kim AM, O'Halloran TV, Woodruff TK. 2012. Zinc
769 maintains prophase I arrest in mouse oocytes through regulation of the MOS-
770 MAPK pathway. *Biol.Reprod*. **87:**11, 1–12. doi:10.1095/biolreprod.112.099390

771 Kong BY, Duncan FE, Que EL, Xu Y, Vogt S, O'Halloran TV, Woodruff TK.
772 2015. The inorganic anatomy of the mammalian preimplantation embryo and
773 the requirement of zinc during the first mitotic divisions. *Dev.Dyn*. **244:**935–947.
774 doi:10.1002/dvdy.24285

775 Lan Z, Xu X, Cooney AJ. 2004. Differential oocyte-specific expression of Cre
776 recombinase activity in GDF-9-iCre, Zp3cre, and Msx2Cre transgenic mice.
777 *Biol.Reprod*. **71:**1469–1474. doi:10.1095/biolreprod.104.031757

778 Lee HC, Edmonds ME, Duncan FE, O'Halloran TV, Woodruff TK. 2020. Zinc
779 exocytosis is sensitive to myosin light chain kinase inhibition in mouse and
780 human eggs. *Mol.Hum.Reprod*. **26:**228–239. doi:10.1093/molehr/gaaa017

781 Lu M, Fu D. 2007. Structure of the zinc transporter YiiP. *Science* **317:**1746–
782 1748. doi:10.1126/science.1143748

783 Lubna S, Ahmad R. 2023. Clinical and biochemical understanding of Zinc
784 interaction during liver diseases: A paradigm shift. *J.Trace Elem.Med.Biol*.
785 **77:**127130. doi:10.1016/j.jtemb.2023.127130

786 Miyai T, Hojyo S, Ikawa T, Kawamura M, Irie T, Ogura H, Hijikata A, Bin B,
787 Yasuda T, Kitamura H, Nakayama M, Ohara O, Yoshida H, Koseki H, Mishima
788 K, Fukada T. 2014. Zinc transporter SLC39A10/ZIP10 facilitates antiapoptotic
789 signaling during early B-cell development. *Proc.Natl.Acad.Sci.U.S.A*.
790 **111:**11780–11785. doi:10.1073/pnas.1323549111

791 Miyazaki S, Yuzaki M, Nakada K, Shirakawa H, Nakanishi S, Nakade S,
792 Mikoshiba K. 1992. Block of Ca2+ wave and Ca2+ oscillation by antibody to the
793 inositol 1,4,5-trisphosphate receptor in fertilized hamster eggs. *Science*
794 **257:**251–255. doi:10.1126/science.1321497

795 Miyazaki S, Ito M. 2006. Calcium signals for egg activation in mammals.
796 *J.Pharmacol.Sci*. **100:**545–552. doi:10.1254/jphs.cpj06003x

797 Nakajima K, Lee M, Bin B, Hara T, Takagishi T, Chae S, Sano S, Fukada T.
798 2020. Possible involvement of zinc transporter ZIP10 in atopic dermatitis.
799 *J.Dermatol*. **47:**e51–e53. doi:10.1111/1346-8138.15190

800 Namiki T, Terakawa J, Karakama H, Noguchi M, Murakami H, Hasegawa Y,
801 Ohara O, Daikoku T, Ito J, Kashiwazaki N. 2023. Uterine epithelial Gp130
802 orchestrates hormone response and epithelial remodeling for successful
803 embryo attachment in mice. *Sci.Rep*. **13:**854–y. doi:10.1038/s41598-023-
804 27859-y

805 Ohe M, Kawamura Y, Ueno H, Inoue D, Kanemori Y, Senoo C, Isoda M, Nakajo
806 N, Sagata N. 2010. Emi2 inhibition of the anaphase-promoting
807 complex/cyclosome absolutely requires Emi2 binding via the C-terminal RL tail.
808 *Mol.Biol.Cell* **21:**905–913. doi:10.1091/mbc.e09-11-0974

809 Paknejad N, Hite RK. 2018. Structural basis for the regulation of inositol
810 trisphosphate receptors by Ca(2+) and IP(3). *Nat.Struct.Mol.Biol*. **25:**660–668.
811 doi:10.1038/s41594-018-0089-6

812 Pal D, Sharma U, Singh SK, Prasad R. 2014. Association between ZIP10 gene
813 expression and tumor aggressiveness in renal cell carcinoma. *Gene* **552:**195–
814 198. doi:10.1016/j.gene.2014.09.010

815 Parrington J, Brind S, De Smedt H, Gangeswaran R, Lai FA, Wojcikiewicz R,
816 Carroll J. 1998. Expression of inositol 1,4,5-trisphosphate receptors in mouse
817 oocytes and early embryos: the type I isoform is upregulated in oocytes and
818 downregulated after fertilization. *Dev.Biol*. **203:**451–461.
819 doi:10.1006/dbio.1998.9071

820 Pascua AM, Nikoloff N, Carranza AC, Anchordoquy JP, Quintana S, Barbisan
821 G, Diaz S, Anchordoquy JM, Furnus CC. 2020. Reproductive hormones
822 influence zinc homeostasis in the bovine cumulus-oocyte complex: Impact on
823 intracellular zinc concentration and transporters gene expression.
824 *Theriogenology* **146:**48–57. doi:10.1016/j.theriogenology.2020.01.054

825 Polanco JC, Wilhelm D, Davidson T, Knight D, Koopman P. 2010. Sox10 gain-
826 of-function causes XX sex reversal in mice: implications for human 22q-linked
827 disorders of sex development. *Hum.Mol.Genet*. **19:**506–516.
828 doi:10.1093/hmg/ddp520

829 Prasad AS. 1996. Zinc deficiency in women, infants and children.
830 J*.Am.Coll.Nutr*. **15:**113–120. doi:10.1080/07315724.1996.10718575

831 Que EL, Bleher R, Duncan FE, Kong BY, Gleber SC, Vogt S, Chen S, Garwin
832 SA, Bayer AR, Dravid VP, Woodruff TK, O'Halloran TV. 2015. Quantitative
833 mapping of zinc fluxes in the mammalian egg reveals the origin of fertilization-
834 induced zinc sparks. *Nat.Chem*. **7:**130–139. doi:10.1038/nchem.2133

835 Que EL, Duncan FE, Bayer AR, Philips SJ, Roth EW, Bleher R, Gleber SC,
836 Vogt S, Woodruff TK, O'Halloran TV. 2017. Zinc sparks induce physiochemical
837 changes in the egg zona pellucida that prevent polyspermy. *Integr.Biol.(Camb)*
838 **9:**135–144. doi:10.1039/c6ib00212a

839 Que EL, Duncan FE, Lee HC, Hornick JE, Vogt S, Fissore RA, O'Halloran TV,
840 Woodruff TK. 2019. Bovine eggs release zinc in response to parthenogenetic
841 and sperm-induced egg activation. *Theriogenology* **127:**41–48.
842 doi:10.1016/j.theriogenology.2018.12.031

843 Saunders CM, Larman MG, Parrington J, Cox LJ, Royse J, Blayney LM, Swann
844 K, Lai FA. 2002. PLC zeta: a sperm-specific trigger of Ca(2+) oscillations in
845 eggs and embryo development. *Development* **129:**3533–3544.
846 doi:10.1242/dev.129.15.3533

847 Schmitt-Ulms G, Ehsani S, Watts JC, Westaway D, Wille H. 2009. Evolutionary
848 descent of prion genes from the ZIP family of metal ion transporters. *PLoS One*
849 **4:**e7208. doi:10.1371/journal.pone.0007208

850 Schmitz C, Sadr SZ, Korschgen H, Kuske M, Schoen J, Stocker W, Jahnen-
851 Dechent W, Floehr J. 2021. The E-modulus of the oocyte is a non-destructive
852 measure of zona pellucida hardening. *Reproduction* **162:**259–266.
853 doi:10.1530/REP-21-0122

854 Seeler JF, Sharma A, Zaluzec NJ, Bleher R, Lai B, Schultz EG, Hoffman BM,
855 LaBonne C, Woodruff TK, O'Halloran TV. 2021. Metal ion fluxes controlling
856 amphibian fertilization. *Nat.Chem*. **13:**683–691. doi:10.1038/s41557-021-00705-
857 2

858 Shoji S, Muto Y, Ikeda M, He F, Tsuda K, Ohsawa N, Akasaka R, Terada T,
859 Wakiyama M, Shirouzu M, Yokoyama S. 2014. The zinc-binding region (ZBR)
860 fragment of Emi2 can inhibit APC/C by targeting its association with the
861 coactivator Cdc20 and UBE2C-mediated ubiquitylation. *FEBS Open Bio* **4:**689–
862 703. doi:10.1016/j.fob.2014.06.010

863 Sugita H, Takarabe S, Kageyama A, Kawata Y, Ito J. 2024. Molecular
864 Mechanism of Oocyte Activation in Mammals: Past, Present, and Future
865 Directions. *Biomolecules* **14:**359. doi: 10.3390/biom14030359.
866 doi:10.3390/biom14030359

867 Suzuki T, Yoshida N, Suzuki E, Okuda E, Perry ACF. 2010. Full-term mouse
868 development by abolishing Zn2+-dependent metaphase II arrest without Ca2+
869 release. *Development* **137:**2659–2669. doi:10.1242/dev.049791

870 Takagishi T, Hara T, Fukada T. 2017. Recent Advances in the Role of
871 SLC39A/ZIP Zinc Transporters In Vivo. *Int.J.Mol.Sci*. **18:**2708. doi:
872 10.3390/ijms18122708. doi:10.3390/ijms18122708

873 Taylor KM, Muraina IA, Brethour D, Schmitt-Ulms G, Nimmanon T, Ziliotto S,
874 Kille P, Hogstrand C. 2016. Zinc transporter ZIP10 forms a heteromer with ZIP6
875 which regulates embryonic development and cell migration. *Biochem.J*.
876 **473:**2531–2544. doi:10.1042/BCJ20160388

877 Tian X, Diaz FJ. 2012. Zinc depletion causes multiple defects in ovarian
878 function during the periovulatory period in mice. *Endocrinology* **153:**873–886.
879 doi:10.1210/en.2011-1599

880 Tokuhiro K, Dean J. 2018. Glycan-Independent Gamete Recognition Triggers
881 Egg Zinc Sparks and ZP2 Cleavage to Prevent Polyspermy. *Dev.Cell*. **46:**627–
882 640.e5. doi:10.1016/j.devcel.2018.07.020

883 Xu Z, Kopf GS, Schultz RM. 1994. Involvement of inositol 1,4,5-trisphosphate-
884 mediated Ca2+ release in early and late events of mouse egg activation.
885 *Development* **120:**1851–1859. doi:10.1242/dev.120.7.1851

886 Xu Z, Williams CJ, Kopf GS, Schultz RM. 2003. Maturation-associated increase
887 in IP3 receptor type 1: role in conferring increased IP3 sensitivity and Ca2+
888 oscillatory behavior in mouse eggs. *Dev.Biol*. **254:**163–171. doi:10.1016/s0012-
889 1606(02)00049-0

890 Yokokawa H, Fukuda H, Saita M, Miyagami T, Takahashi Y, Hisaoka T, Naito T.
891 2020. Serum zinc concentrations and characteristics of zinc deficiency/marginal
892 deficiency among Japanese subjects. *J.Gen.Fam.Med*. **21:**248–255.
893 doi:10.1002/jgf2.377

894 Yoon S, Fissore RA. 2007. Release of phospholipase C zetaand [Ca2+]i
895 oscillation-inducing activity during mammalian fertilization. *Reproduction*
896 **134:**695–704. doi:10.1530/REP-07-0259

897

898

899

900

901 **Figure legends**

902 **Fig. 1. Expression of ZIP6 and ZIP10 in mouse ovary. (A**) In situ hybridization
903 in the mouse ovary showed ZIP10 expression in oocyte and granulosa cell from
904 primordial, primary, secondary and antral follicle. Arrow indicates primordial
905 follicular oocyte. (**B**) Immunofluorescent staining for ZIP10 (green) in the mouse
906 ovary showed ZIP10 expression in oocyte membrane. Arrow indicates primordial
907 follicular oocyte. (**C**) Immunofluorescent staining for ZIP6 (green) in the mouse
908 ovary showed ZIP6 expression in oocyte nucleus and granulosa cells. Arrow
909 indicates primordial follicular oocyte. (**D**) Immunofluorescent staining showed
910 ZP2 (green; zona pellucida) and FOXL2 (red; granulosa cells) in the mouse ovary.
911 ZP2 was not stain in primordial follicle, but primary, secondary and antral follicles
912 stained. FOXL2 observed at granulosa cells of all stage follicles. The scale bar
913 represents 20 μm of primordial-secondary follicle and 150 μm of antral follicle (**A-**
914 **D**).

915

916 **Fig. 2 Number of collected oocytes and dynamics of labile zinc ion in**
917 ***Zip10$^{d/d}$* mice.** (**A**) The results of average number of oocytes in each group. Data
918 represents the average ± SEM. These experiments were repeated at least thrice.
919 Statistical differences were calculated according to student's *t*-test ($p > 0.05$; no
920 significant difference). (**B**) The percentage of extrusion of first polar body at 10,
921 12 and 14 h after IVM. These experiments were repeated at least thrice.
922 Statistical differences were calculated according to student's *t*-test ($p > 0.05$; no
923 significant difference). (**C**) The morphology of spindle and chromosome
924 organization in *Zip10$^{f/f}$* and *Zip10$^{d/d}$* MII oocytes at 14 h after IVM. Anti–α-tubulin

925 antibody (green) was used to stain the spindles. Chromosomes were stained with
926 DAPI (blue). The scale bar represents 10 μm. (**D**) Comparison with the
927 fluorescence intensity of intracellular labile zinc ion in GV, MII and 2PN. The
928 upper images showed the fluorescence of intracellular labile zinc ion of oocyte or
929 embryo treated with 2 μM FluoZin-3AM for 1h. Representative images are shown.
930 The white dotted circles indicate the positions of oocytes and embryos. Scale
931 bars denote 10 μm. The lower part showed the fluorescence intensity of labile
932 zinc ions in oocytes or embryos. Data represent the average ± SE of the
933 experiments. For each experiment, 10–20 oocytes/embryos were stained and
934 used for the measurement in each stage of the experiment, and these
935 experiments were repeated three times. Statistical differences were calculated
936 according to the welch's *t*-test. Different letters represent significant differences
937 ($p < 0.05$).
938
939 **Fig. 3 Measurement of calcium spike and zinc spark in *Zip10$^{d/d}$* mice.** (**A**)
940 The representative images of before or after IVF in mouse oocytes. Left side
941 images showed before fertilization. Right side images showed after fertilization.
942 The oocytes increased calcium ion and released zinc ion shortly after fertilization.
943 The white dotted circles indicate the positions of oocytes. Successful fertilization
944 was confirmed by simultaneously monitoring intracellular calcium oscillations with
945 Calbryte 590 AM and excellular zinc ions with FluoZin-3 every 4 s. Capacitated
946 frozen-thawed sperm was added to MII at 2 min after imaging start. Orange line
947 showed calcium ion and dark blue line showed zinc ion. Intracellular calcium
948 increases immediately before a zinc spark. Scale bars denote 20 μm. (**B**) The
949 representative images of an MII egg activated with 5 μM ionomycin followed by
950 monitoring of intracellular calcium oscillations with Calbryte 590 AM and
951 extracellular zinc using 20 μM FluoZin-3. The ionomycin was added to MII at 2
952 min after imaging start. Orange line showed calcium ion and dark blue line
953 showed zinc ion. Intracellular calcium increases immediately before a zinc spark.
954 Scale bars denote 20 μm.
955
956 **Fig. 4 Presence of a mechanism to prevent multisperm fertilization in Zip10**

957 **cKO mice.** (**A**) The percentages of oocytes with each number of PN at 6 h after
958 insemination. Yellow region showed other including degeneration, degression
959 and fragmentation. Gray region showed unfertilization, namely MII oocytes.
960 Orange showed 2PN2PB, namely embryo possessed one female and male
961 pronucleous (2PN) and second polar body (2PB). Blue region showed multisperm
962 fertilization (3PN2PB). (**B**) The percentage of fertilized oocytes and
963 developmental embryos. Data represent the average ± SE of the experiments.
964 The embryo development was observed at 6 (2PN) 24 (2 cell), 48 (4-8 cell), 72
965 (Morula), and 96 (Blastocyst) hours after IVF. The oocytes used for IVF were
966 calculated as the parameter for the fertilization rate and the rate of embryo
967 development. These experiments were repeated at least thrice. Statistical
968 differences were calculated according to the chi-square test. Different letters
969 represent significant differences ($p < 0.05$). (**C**) The cell number of blastocyst
970 derived from IVF. Blastocysts were fixed, immunostained, and physically
971 flattened between a slide and coverslip. Photographs represent a single plane of
972 focus. Nuclei are indicated by DAPI staining. The count used inverted
973 fluorescence microscope. These experiments were repeated three times, and
974 each group counted total 46 embryos. Statistical differences were calculated
975 according to the student's *t*-test ($p < 0.05$; significant difference). (**D**) Western blot
976 of oocytes from *Zip10*$^{f/f}$ and *Zip10*$^{d/d}$ mice at 0 or 6 h after insemination using rat
977 anti-ZP2 antibody. Intact ZP2 and the cleaved C-terminal fragment of ZP2
978 measured 120-130 kD and undetected, respectively. Expression level of β-actin
979 serves as a protein loading control. Molecular mass is indicated at the left. (**E**) MII
980 oocytes and 2PN embryos from *Zip10*$^{f/f}$ and *Zip10*$^{d/d}$ mice were imaged by
981 confocal microscopy after staining with rabbit anti-ovastacin (green).
982 Chromosomes were stained with DAPI (blue). The scale bar represents 10 μm.
983 (**F**) MII oocytes and 2PN embryos from *Zip10*$^{f/f}$ and *Zip10*$^{d/d}$ mice were imaged by
984 BZ-X700 microscopy after staining with rat anti-mouse FR4 (JUNO; green).
985 Chromosomes were stained with DAPI (blue). The scale bar represents 10 μm.
986
987 **Movie legends**
988 **Movie 1. Monitoring of intracellular calcium ions during fertilization of**

989 ***Zip10$^{f/f}$* oocytes.** The changes in Ca^{2+} were detected by CalbryteTM 590 AM
990 every 4 second. *Zip10$^{f/f}$* oocytes displayed the calcium oscillations following
991 fertilization. The changes in zinc ions were also monitored simultaneously (Movie
992 2). The video was excerpted from maximum 50 min.
993
994 **Movie 2. Monitoring of extracellular zinc ions during fertilization of *Zip10$^{f/f}$***
995 **oocytes.** The changes in Zn^{2+} were detected by FluoZin-3 every 4 second.
996 *Zip10$^{f/f}$* oocytes released zinc ions into the extracellular environment through a
997 zinc spark followed the first calcium rise following fertilization. The changes in
998 calcium ions were also monitored simultaneously (Movie 1). The video was
999 excerpted from maximum 50 min.
1000
1001 **Movie 3. Monitoring of intracellular calcium ions during fertilization of**
1002 ***Zip10$^{d/d}$* oocytes.** The changes in Ca^{2+} were detected by CalbryteTM 590 AM
1003 every 4 second. *Zip10$^{d/d}$* oocytes displayed the calcium oscillations following
1004 fertilization. The changes in zinc ions were also monitored simultaneously (Movie
1005 4). The video was excerpted from maximum 50 min.
1006
1007 **Movie 4. Monitoring of extracellular zinc ions during fertilization of *Zip10$^{d/d}$***
1008 **oocytes.** The changes in Zn^{2+} were detected by FluoZin-3 every 4 second.
1009 *Zip10$^{d/d}$* oocytes did not release zinc ions into the extracellular environment
1010 followed the first calcium rise following fertilization. The changes in calcium ions
1011 were also monitored simultaneously (Movie 3). The video was excerpted from
1012 maximum 50 min.
1013
1014 **Movie 5. Monitoring of intracellular calcium ions during parthenogenesis of**
1015 ***Zip10$^{f/f}$* oocytes.** The changes in Ca^{2+} were detected by CalbryteTM 590 AM
1016 every 4 second. *Zip10$^{f/f}$* oocytes displayed a transient rise of calcium ions
1017 following artificial oocyte activation with ionomycin. The changes in zinc ions were
1018 also monitored simultaneously (Movie 6). The video was excerpted from
1019 maximum 50 min.
1020

1021 **Movie 6. Monitoring of extracellular zinc ions during parthenogenesis of**
1022 ***Zip10$^{f/f}$* oocytes.** The changes in Zn^{2+} were detected by FluoZin-3 every 4
1023 second. *Zip10$^{f/f}$* oocytes released zinc ions into the extracellular environment
1024 through a zinc spark followed a transient calcium rise following artificial oocyte
1025 activation with ionomycin. The changes in calcium ions were also monitored
1026 simultaneously (Movie 5). The video was excerpted from maximum 50 min.
1027
1028 **Movie 7. Monitoring of intracellular calcium ions during parthenogenesis of**
1029 ***Zip10$^{d/d}$* oocytes.** The changes in Ca^{2+} were detected by CalbryteTM 590 AM
1030 every 4 second. *Zip10$^{d/d}$* oocytes displayed a transient rise of calcium ions
1031 following artificial oocyte activation with ionomycin. The changes in zinc ions were
1032 also monitored simultaneously (Movie 8). The video was excerpted from
1033 maximum 50 min.
1034
1035 **Movie 8. Monitoring of extracellular zinc ions during parthenogenesis of**
1036 ***Zip10$^{d/d}$* oocytes.** The changes in Zn^{2+} were detected by FluoZin-3 every 4
1037 second. *Zip10$^{d/d}$* oocytes did not release zinc ions into the extracellular
1038 environment followed a transient calcium rise following artificial oocyte activation
1039 with ionomycin. The changes in calcium ions were also monitored simultaneously
1040 (Movie 5). The video was excerpted from maximum 50 min.
1041
1042
1043
1044
1045
1046
1047
1048
1049
1050
1051
1052

1053

1054

1055

1056

1057

Fig. 1.

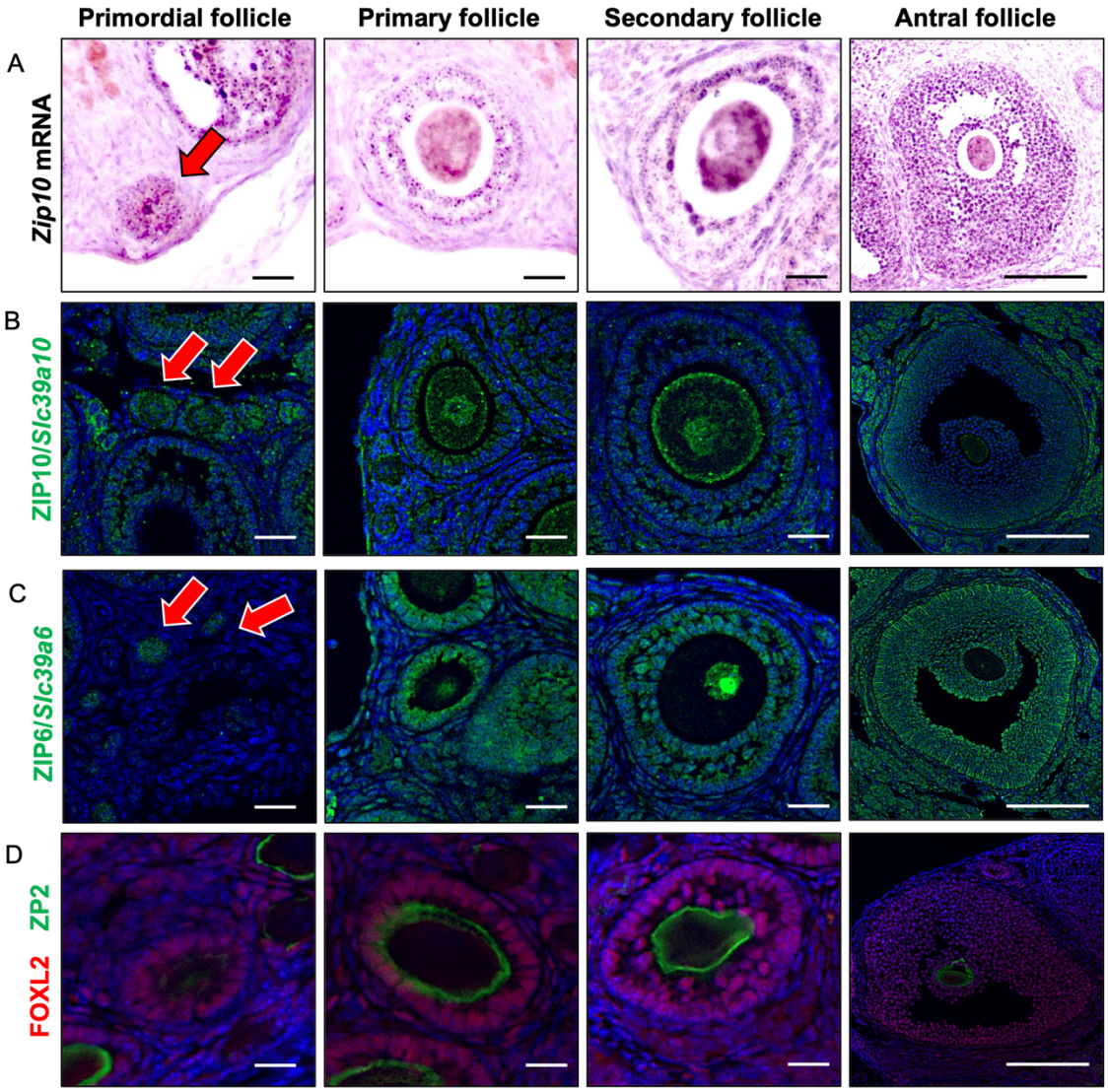

1058

1059

1060

1061

1062

1063

1064

1065

Fig. 2.

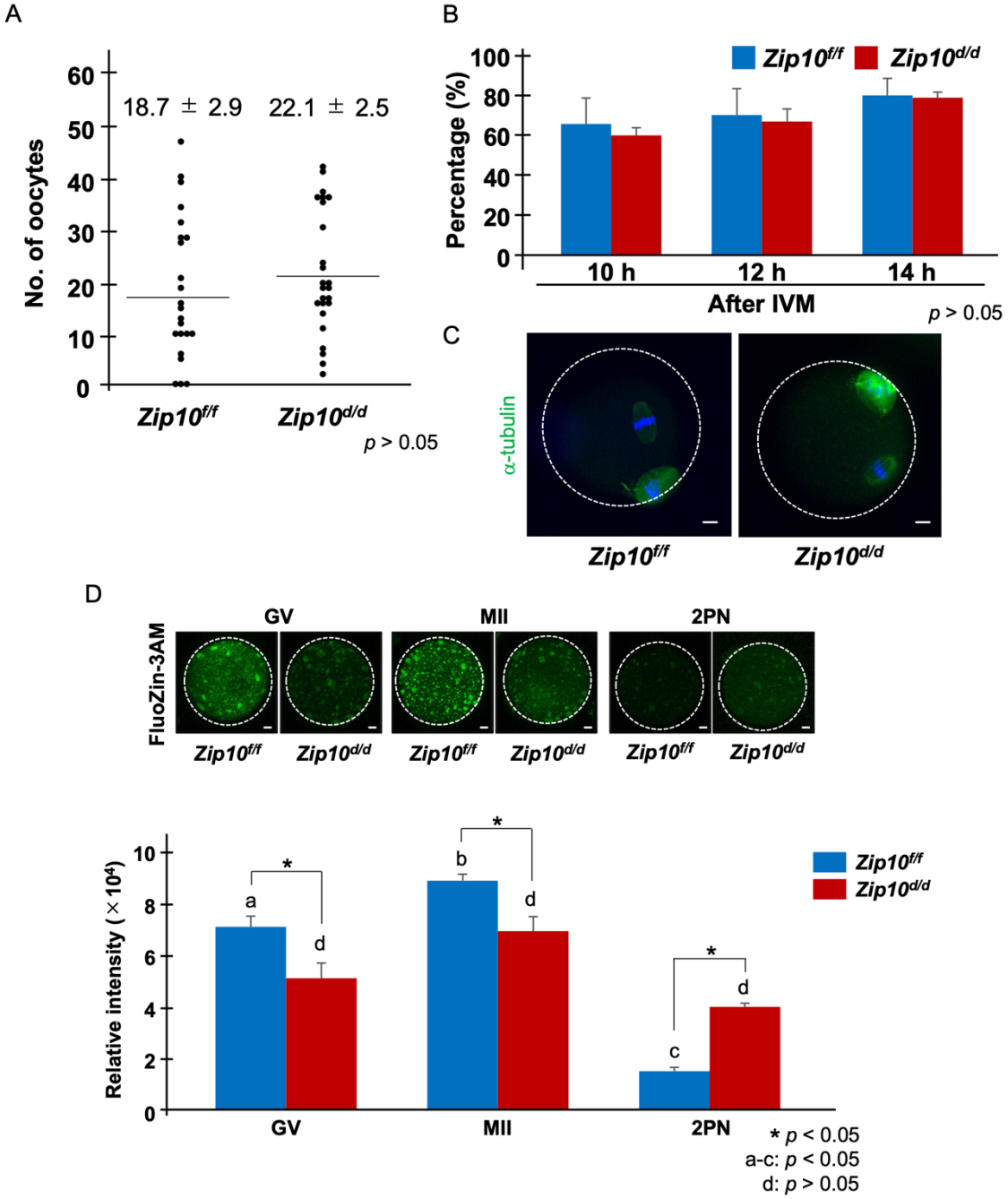

1066

1067

1068

1069

Fig. 3.

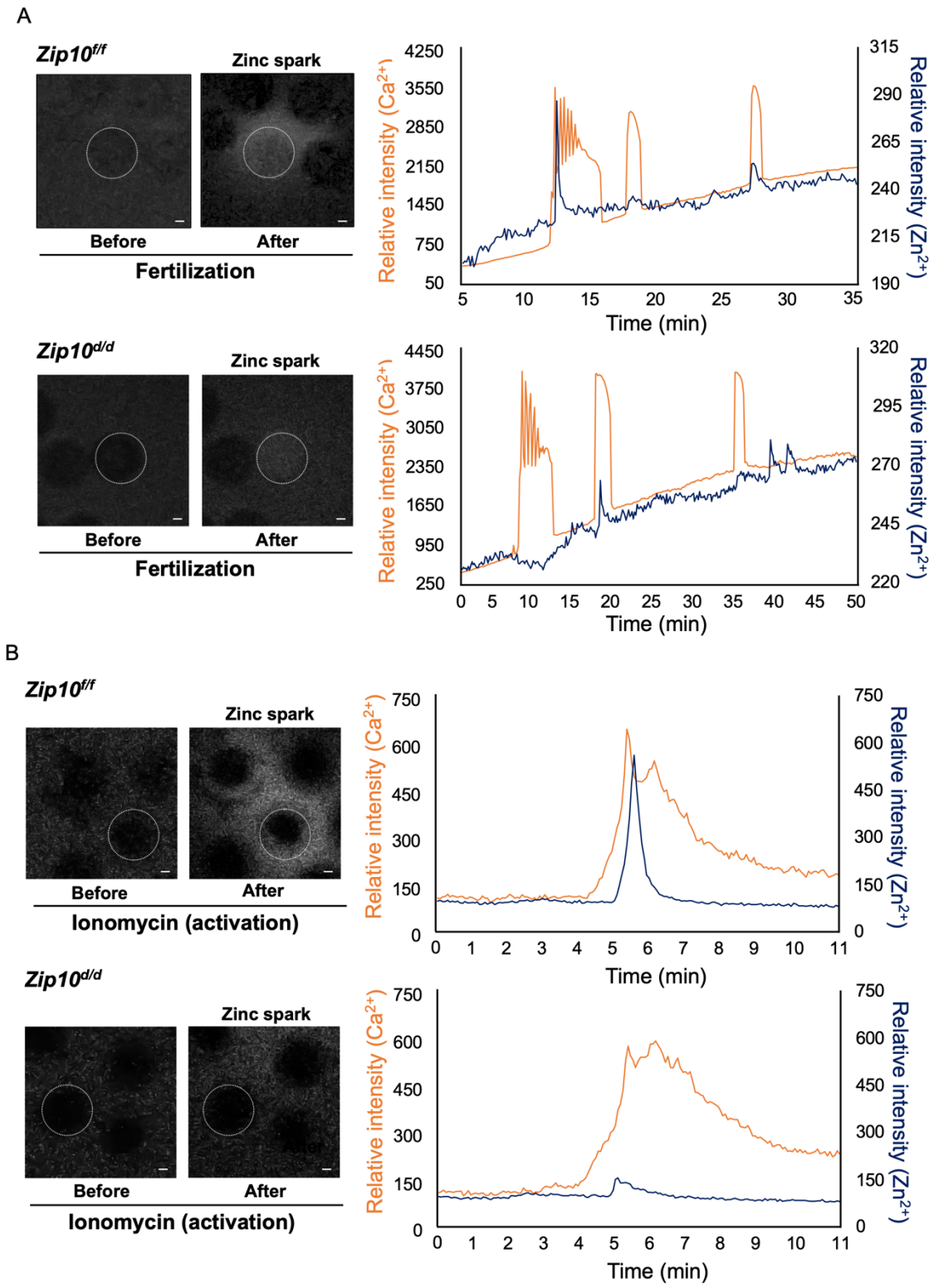

1070

1071

1072

Fig. 4.

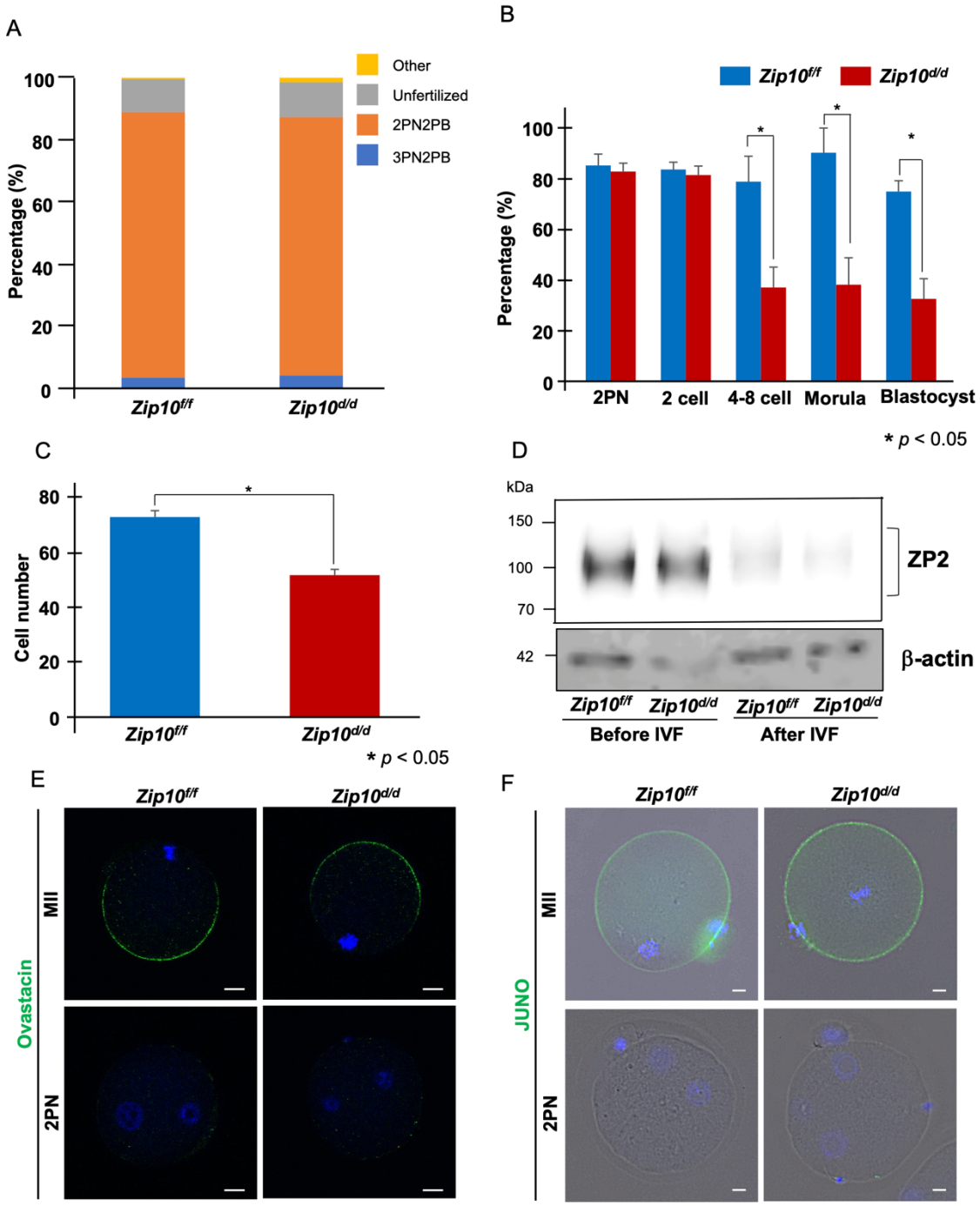

1073

1074